ARTICLE

www.the-innovation.org

A piezoelectric-driven microneedle platform for skin disease therapy

Ziyan Chen,[1,2,3,7,11] Xin Liu,[1,2,3,4,5,6,8,11] Zixi Jiang,[1,2,3,4,5,6,11] Huayi Wu,[2,3,7] Tao Yang,[9] Lanyuan Peng,[1,2,3,4,5,6] Lisha Wu,[1,2,3,4,5,6] Zhongling Luo,[1,2,3,4,5,6] Mi Zhang,[1,2,3,4,5,6] Juan Su,[1,2,3,4,5,6] Yan Tang,[1,2,3,4,5,6] Jinmao Li,[1,2,3,4,5,6] Yang Xie,[2,3,7] Han Shan,[2,3,7] Qibo Lin,[2,3,7] Xiuli Wang,[10] Xiang Chen,[1,2,3,4,5,6] Hanmin Peng,[9,*] Shuang Zhao,[1,2,3,4,5,6,*] and Zeyu Chen[1,2,3,7,*]

*Correspondence: penghm@nuaa.edu.cn (H.P.); shuangxy@csu.edu.cn (S.Z.); zeyuchen@csu.edu.cn (Z.C.)

Received: November 23, 2023; Accepted: March 29, 2024; Published Online: April 5, 2024; https://doi.org/10.1016/j.xinn.2024.100621

GRAPHICAL ABSTRACT

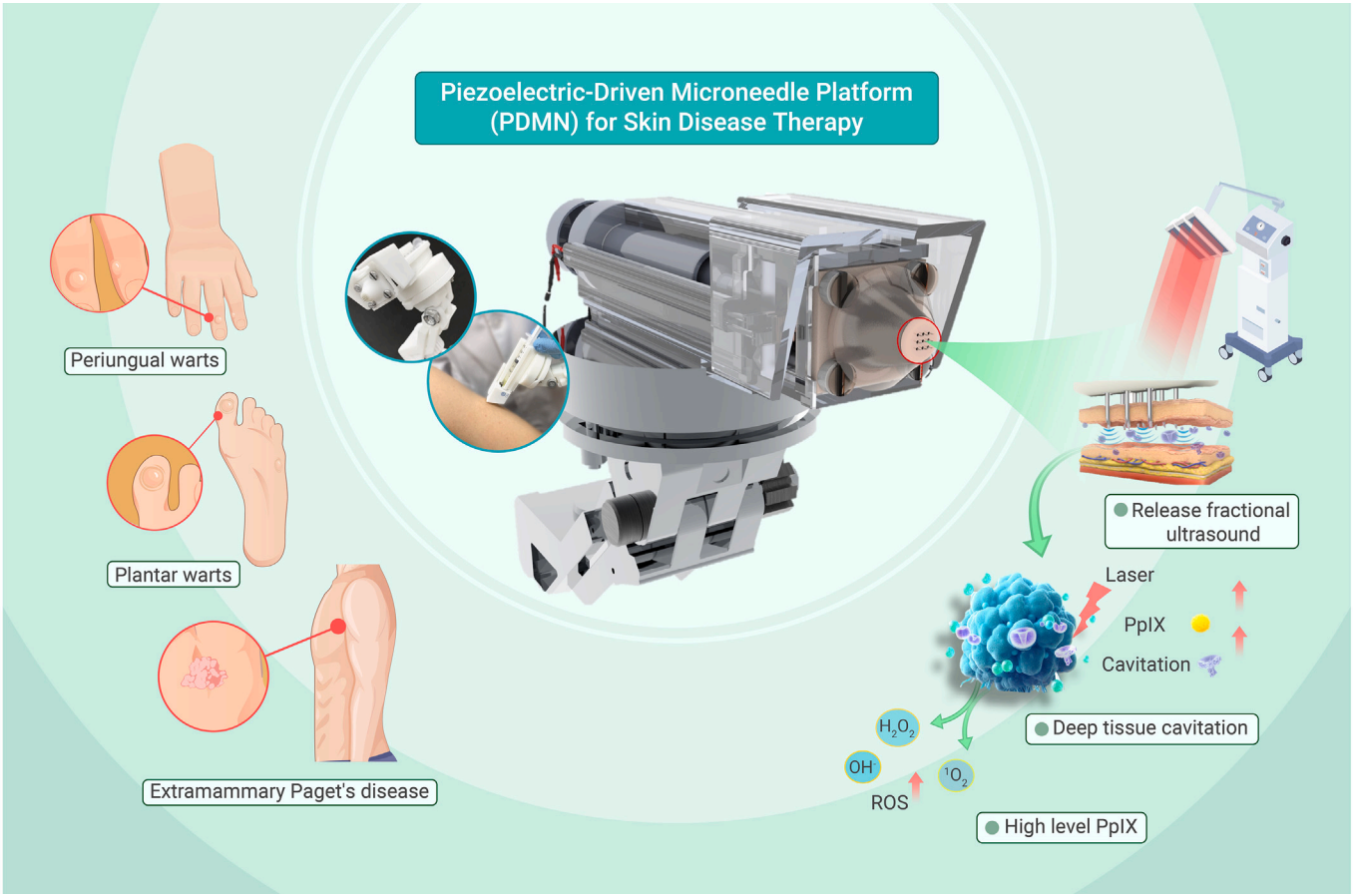

PUBLIC SUMMARY

- Piezoelectric-driven microneedle (PDMN) platform is fabricated for deep tissue cavitation with high-level reactive oxygen species.
- PDMN significantly enhances transdermal drug delivery in a minimally invasive manner.
- PDMN platform achieves a deeper penetration depth of the photosensitizer and higher accumulation of photosensitizers in tumor compared to traditional photodynamic therapy (PDT) in animal models.
- Clinical trials demonstrated that PDMN-PDT not only boosted treatment effectiveness with high patient compliance but also remarkably reduced the treatment time and drug concentration.

ARTICLE

A piezoelectric-driven microneedle platform for skin disease therapy

Ziyan Chen,[1,2,3,7,11] Xin Liu,[1,2,3,4,5,6,8,11] Zixi Jiang,[1,2,3,4,5,6,11] Huayi Wu,[2,3,7] Tao Yang,[9] Lanyuan Peng,[1,2,3,4,5,6] Lisha Wu,[1,2,3,4,5,6] Zhongling Luo,[1,2,3,4,5,6] Mi Zhang,[1,2,3,4,5,6] Juan Su,[1,2,3,4,5,6] Yan Tang,[1,2,3,4,5,6] Jinmao Li,[1,2,3,4,5,6] Yang Xie,[2,3,7] Han Shan,[2,3,7] Qibo Lin,[2,3,7] Xiuli Wang,[10] Xiang Chen,[1,2,3,4,5,6] Hanmin Peng,[9,*] Shuang Zhao,[1,2,3,4,5,6,*] and Zeyu Chen[1,2,3,7,*]

[1]Department of Dermatology, Xiangya Hospital, Central South University, Changsha 410008, China
[2]Furong Laboratory (Precision Medicine), Changsha 410008, China
[3]National Engineering Research Center of Personalized Diagnostic and Therapeutic Technology, Xiangya Hospital, Central South University, Changsha 410008, China
[4]Hunan Engineering Research Center of Skin Health and Disease, Xiangya Hospital, Central South University, Changsha 410008, China
[5]Hunan Key Laboratory of Skin Cancer and Psoriasis, Xiangya Hospital, Central South University, Changsha 410008, China
[6]National Clinical Research Center of Geriatric Disorders, Xiangya Hospital, Central South University, Changsha 410008, China
[7]School of Mechanical and Electrical Engineering, Central South University, Changsha 410083, China
[8]Department of Dermatology, Xijing Hospital, The Fourth Military Medical University, Xi'an, Shaanxi 710000, China
[9]State Key Laboratory of Mechanics and Control for Aerospace Structures, Nanjing University of Aeronautics & Astronautics, Nanjing 210016, China
[10]Institute of Photomedicine, Shanghai Skin Disease Hospital, School of Medicine, Tongji University, Shanghai 200443, China
[11]These authors contributed equally
*Correspondence: penghm@nuaa.edu.cn (H.P.); shuangxy@csu.edu.cn (S.Z.); zeyuchen@csu.edu.cn (Z.C.)

Received: November 23, 2023; Accepted: March 29, 2024; Published Online: April 5, 2024; https://doi.org/10.1016/j.xinn.2024.100621

Citation: Chen Z., Liu X., Jiang Z., et al., (2024). A piezoelectric-driven microneedle platform for skin disease therapy. The Innovation **5(3)**, 100621.

With over a million cases detected each year, skin disease is a global public health problem that diminishes the quality of life due to its difficulty to eradicate, propensity for recurrence, and potential for post-treatment scarring. Photodynamic therapy (PDT) is a treatment with minimal invasiveness or scarring and few side effects, making it well tolerated by patients. However, this treatment requires further research and development to improve its effective clinical use. Here, a piezoelectric-driven microneedle (PDMN) platform that achieves high efficiency, safety, and non-invasiveness for enhanced PDT is proposed. This platform induces deep tissue cavitation, increasing the level of protoporphyrin IX and significantly enhancing drug penetration. A clinical trial involving 25 patients with skin disease was conducted to investigate the timeliness and efficacy of PDMN-assisted PDT (PDMN-PDT). Our findings suggested that PDMN-PDT boosted treatment effectiveness and reduced the required incubation time and drug concentration by 25% and 50%, respectively, without any anesthesia compared to traditional PDT. These findings suggest that PDMN-PDT is a safe and minimally invasive approach for skin disease treatment, which may improve the therapeutic efficacy of topical medications and enable translation for future clinical applications.

INTRODUCTION

The skin is the largest organ, covering approximately 16% of total body mass. Skin conditions represent a significant part of the global total of diseases and can result in significant disfigurement, leading to physical and emotional adverse consequences for patients.[1–3] Photodynamic therapy (PDT) is a painless and non-invasive treatment that is typically used in the treatment of non-melanomatous skin cancers (e.g., Bowen's disease [BD], basal cell carcinoma, and squamous cell carcinoma) and several solid tumor types (non-small cell lung cancer, esophageal cancer, and bladder cancer).[4–10] It offers advantages over alternative treatments such as surgical removal and curettage, which are currently employed in the treatment of skin lesions, including the avoidance of damage to surrounding tissue and minimal or no scarring.[11–14]

Despite favorable outcomes having been reported in many clinical trials, the PDT method still suffers from penetration-limiting properties of the photosensitizer (PS), which ultimately leads to a lack of reactive oxygen species (ROSs) in cancer cells, especially in deeper lesions.[15–17] Clinically, PDT usually begins with topical application of a PS (such as 5-aminolevulinic acid [5-ALA], 20% solutions) followed by at least a 4-h incubation period, which leads to an economic burden and poor patient experience.[15,18] Recently, great progress has been made to enhance therapeutic efficacy including the use of nanocarriers,[19–21] microneedle patches,[22–25] and electroporation.[26] Among these, PS, along with other chemically auxiliary formulations drugs capable of generating ROS were loaded into microneedles to enhance the penetration depth.[27,28] Electroporation techniques apply a strong electric field to create transdermal pathways in skin tissue, and their use in combination with PDT also demonstrates promising therapeutic effects. However, low drug utilization of nanocarriers, the cumbersome preparation processes of microneedle patch, and the tissue damage of electroporation, make PDT still need innovative combined modalities to be applied in clinic.

Thus, in this study, we developed a piezoelectric-driven microneedle (PDMN) platform for physical regulation of the tumor microenvironment via deeper dermis cavitation and enhanced PS delivery for highly effective PDT. PDMN-platform-mediated PDT increased the local protoporphyrin IX (PpIX) level in lesions, which further kills malignant cells, shuts down the tumor microvasculature, and stimulates the host immune system (Figure 1A). The PDMN platform leverages ultrasound (US), which has been widely utilized in clinical settings and is considered one of the safest available devices. A piezoelectric material is utilized to generate an acoustic field, achieving low-density and safe acoustic cavitation, and a specially designed microneedle array (MA) patch with multimicrochannels fabricated using a high-precision three-dimensional (3D) printing technology achieves skin-acoustic coupling and drug delivery (Figure 1B). The PDMN creates a special acoustic field to scatter US and achieve deep tissue cavitation, which leverages the efficiency and safety delivery of PSs and demonstrates a significant accumulation of ROSs at the lesions rather than the skin surface and blood.

RESULTS

PDMN design and principle

PDMN is composed of an MA patch, two pieces of piezo sheets with two copper electrodes, a backing, and an injection connecting tube. The piezoceramic (PZT-8, d_{33}) is used as the PDMN generator (thickness, 2 mm) due to its higher mechanical quality factor, and the adjacent PZT sheets are assembled with opposite polarization directions to achieve superposition. The PDMN platform consists of a PDMN probe and a movable base, with its probe mounted on a multi-degree-of-freedom movable base, allowing for application at multiple angles. This additional structure ensures easy operation and fixation (Figure 1C). Additionally, a designed MA patch with multimicrochannels fabricated by using a high-precision 3D printing technology achieves the installation of microneedles (Figure 2A). The openings of the microchannels can be customized on different heights of the MA, which used to match microneedles of different lengths to achieve acoustic cavitation at different depths. To ensure minimal tissue damage, the microneedle has an outer diameter of only 185 μm and an inner diameter of 120 μm. The height and needle pitch of the microneedles was 1 mm arrayed in a 3 × 3 matrix on a circular base. The area of the microneedle matrix can be adjusted according to the size of the lesion. The efficiency of this platform is exhibited by the measured impedance and phase angle spectra, which show excellent piezoelectricity (Figure 2B). The power intensity (3 W/cm^2) with 30-min operating time and excitation voltage of 200 Vpp indicated that PDMN can create cavitation in a safe manner (Figure 2C). We measured the compressive force under a vertical displacement of the end of the PDMN that was increasing from 0 to

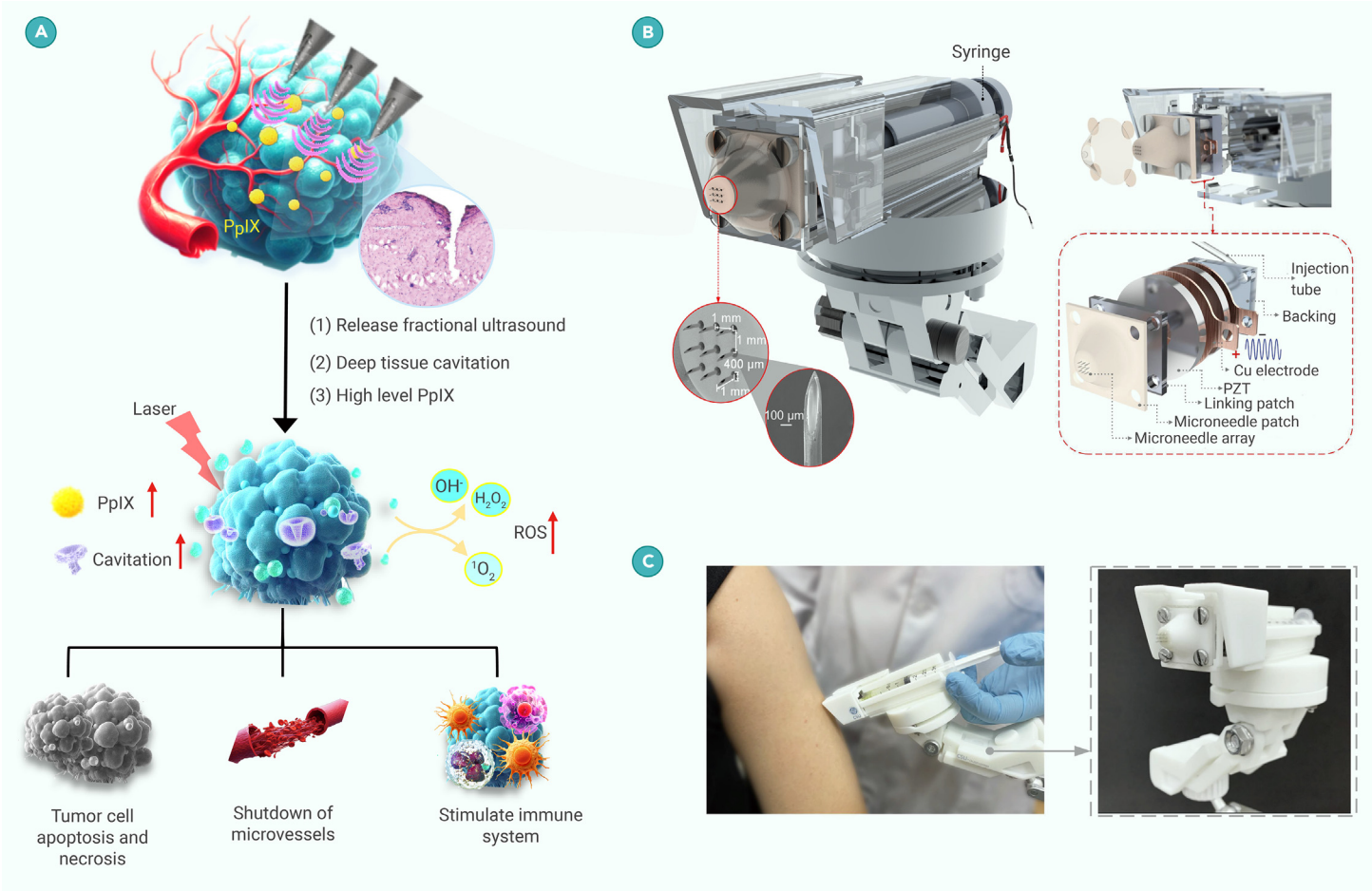

Figure 1. Design and mechanism of PDMN-PDT for skin disease therapy (A) Schematic illustration of PDMN-PDT in lesions. (B) Schematic diagram depicting the structure of PDMN (left). Exploded view of the PDMN (right). (C) Picture of PDMN delivery system for flexible operation.

5 N, and the force was reduced by half under US (Figures 2D and S1). Additionally, we evaluated the thermal effect of PDMN using an infrared thermal camera for 30 min (Figure S2; Video S1). The tissue heats up due to the absorption of US energy and heat transfer from the PDMN. Due to the high thermal conductivity of the piezoceramic and metal, the primary heat generation is produced by PZT and copper. The temperature of the tumor and the contact surface of the PDMN both were maintained around 30°C, and the temperature increase generated by PDMN (5°C) did not cause a bioeffect or associated safety issues (Figure 2E).

We then used the finite element method to simulate the acoustic field and stress field under different skin treatments with US based on a hyperelastic model,[29–31] which took the influence of elastic and collagen fibers in the dermal layer of the skin into consideration (Figure S3). The internal dermal stress under PDMN was close to that in the natural state; simultaneously, the strongest region of the acoustic field intensity was at the depth of the microneedle tip, allowing for dermal cavitation (Figure 2F). Histological findings revealed that the use of PDMN induced cavitation in the deep layer of the dermis, allowing the observation of porous structures (Figure 2G). Similar results were obtained when this experiment was repeated (Figure S4).

PDMN for efficient transdermal drug delivery *in vitro*

To verify the effect of PDMN on PS transdermal delivery, experiments were conducted using excised porcine skin and methylene blue (MB) as a model drug *in vitro*. MB was selected as the model drug because its poor lipid solubility causes it to have difficulty penetrating the skin.[32,33] For comparison, five skin treatments were conducted: untreated skin (Untreated), US treatment with skin compression (US/skin), US treatment without skin compression (US-skin), MA-treated skin (MA), and PDMN-treated skin (PDMN) (Figure S5). Histological assessments (Figure 3A) revealed that regardless of the presence of the MA, skin compression by the US transducer did not cause significant structural changes in the dermis. In contrast, when the transducer was not in contact with the skin, a porous structure caused by cavitation appeared (US-skin and PDMN). These results confirmed the accuracy of the model analysis, which suggested that the internal stresses generated during dermal compression suppress cavitation. Consistent with the model analysis, the maximum intensity of the acoustic field strength in US-skin was located at the skin surface, leading to the formation of a cavitation-induced porous structure at the surface. However, this structure hindered the transmission of US waves to deeper tissues (Figure S3); therefore, we could not observe porous structures in the deeper dermal tissues. Similar to the predictions, PDMN successfully mediated cavitation without increasing the internal stress (PDMN group). Simultaneously, the strongest region of the acoustic field intensity was at the depth of the needle tip, allowing the observation of porous structures caused by cavitation from the skin surface to the depth of the needle tip. Therefore, the PDMN platform may be a promising method for efficient drug delivery by inducing cavitation to increase the interstitial space within the dermis. The skin samples were cut and the cross-sections were observed under a microscope post-treatment. The collected images were processed and enhanced to visualize drug diffusion (Figure 3B). 2D slices showed that, compared to the Untreated group, the US group had more drug penetration through the stratum corneum. Because of the cavitation-induced porous structure in the US group, a greater drug volume was delivered to the upper dermis. In the US group, the dermis formed a significant barrier to drug diffusion. In the MA group, the drug entered the dermis through the microchannels; however, the horizontal diffusion was not obvious. In the PDMN group, drug diffusion was significant in both the vertical and horizontal directions. We also investigated the drug diffusion over time under different power voltages (Figure S6). To avoid sampling bias inherent in 2D slicing, we employed transient-triplet-differential (TTD) method-based photoacoustic imaging to perform 3D scanning reconstruction of the spatial distribution of the drugs in *ex vivo* porcine skin.[34] The resulting images were then sliced horizontally and vertically to

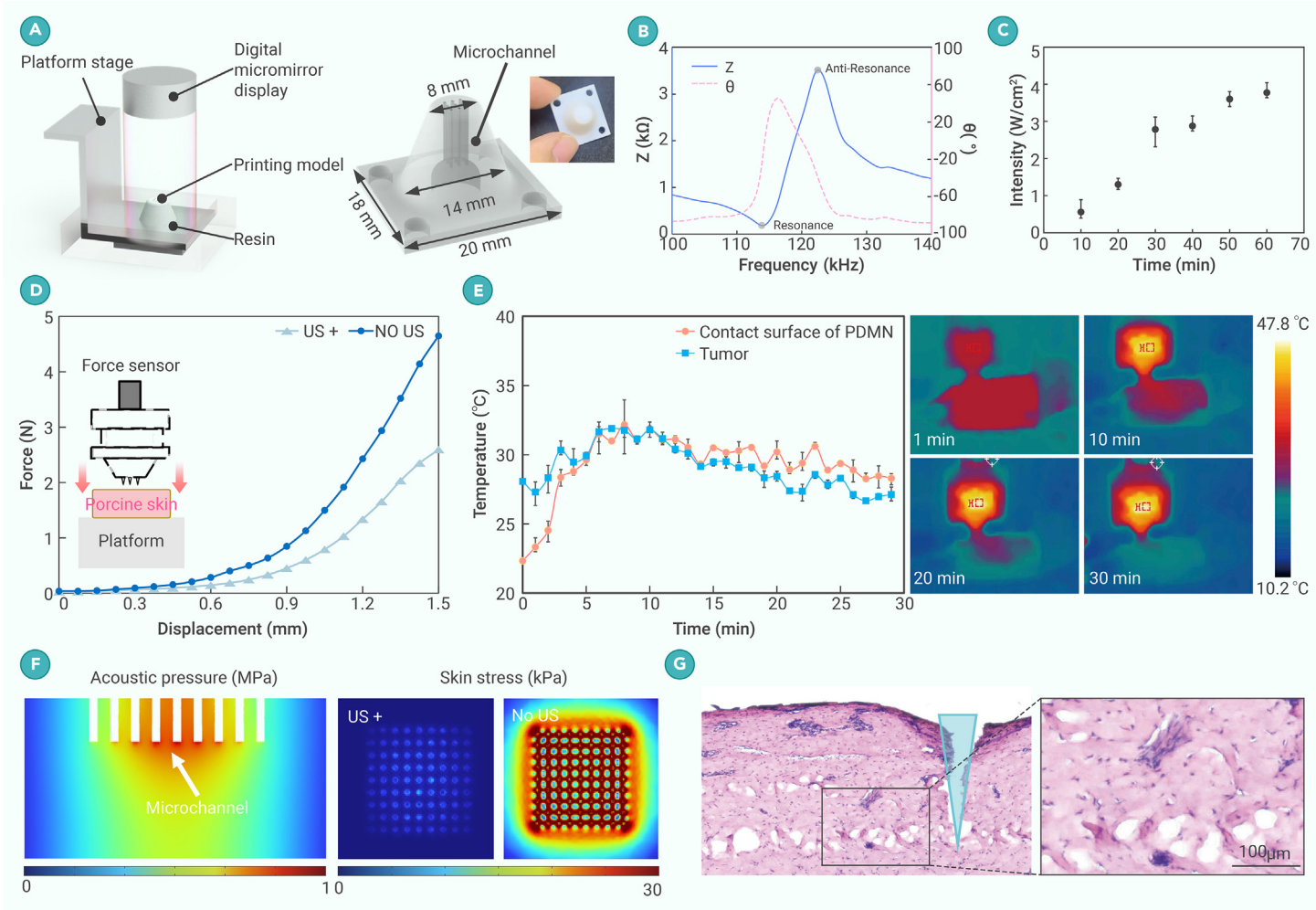

Figure 2. Characterization of the PDMN platform (A) Schematic diagram of the fabrication process of the MA patch by surface projection microstereolithography. (B) Impedance and phase angle spectra of PDMN. The impedance experiment is performed showing PDMN's excellent piezoelectricity. At the resonant frequency, the generator will be the most power efficient. Impedance and phase angle spectra of the PDMN probe after integration showing a center frequency of 114 kHz, an anti-resonance frequency of 122.5 kHz, a phase angle of 80°, and an electromechanical coupling factor k_t of 0.53. (C) Correlation between intensity and time. (D) Mechanical behavior of PDMN against compressive deformation. (E) Temperature changes of PDMN operated for 30 min measured by an infrared thermal camera. Time-temperature curves (left) and representative temperature profiles were captured by a thermal camera every 10 min (right). (F) Finite element method simulation of acoustic pressure and stress field under the skin coupled with PDMN. (G) Representative H&E staining images of porcine skin under PDMN treatments. Scale bar, 100 μm.

analyze drug diffusion in different regions (Figures 3C and 3D; Videos S2, S3, S4, S5, and S6). The results of 3D reconstruction were consistent with those of the 2D slices, suggesting that the PDMN platform had high drug permeation efficiency.

PDMN for efficient 5-ALA delivery and mediated PDT in A431 murine models

Next, we investigated the transdermal delivery efficacy of PDMN *in vivo* in a tumor-bearing mouse model. 5-ALA is the precursor to the PS PpIX, which has been approved by the US Food and Drug Administration in PDT of various dermatological diseases. After a period of incubation, PpIX is generated, which generates cytotoxic ROSs to induce tumor cell death under light illumination (Figure S7). However, the efficacy of PDT is often compromised by its limited route of administration, which results in insufficient penetration of 5-ALA and inadequate production of PpIX. In this study, we first tested the PpIX levels in tumor-bearing mouse skin under two transdermal permeation conditions: topical application and PDMN (Figure 4A). Using a fluorescence microscope, differences in PpIX levels were observed between the two groups at different incubation times (0.5, 1, 1.5, 2, and 4 h) (Figure 4B). After 1.5 h of incubation, PpIX had a diffusion depth of 0.2 mm in the dermis of the topical application group, whereas in the PDMN group, the diffusion depth of PpIX was more than 1.5 mm in the dermis. These findings demonstrated that PDMN-induced dermal cavitation significantly enhanced the transdermal permeation efficiency *in vivo*, which is consistent with the findings of previous *in vitro* experiments. Additionally, we measured the PpIX levels in the tumors, skin, and blood after 4 h of incubation. After 4 h of incubation, the PpIX levels in the tumors were 6 times that of the skin, while in the PDMN group, they were 21 times that of the skin, which resulted in a notable accumulation of PpIX within the tumor, substantially enhancing drug utilization (Figure 4C). These results suggest that the PDMN produces higher levels of PpIX and more accumulated ROSs, which may contribute to the better curative effect and perceived pain levels of PDMN-assisted PDT (PDMN-PDT) due to the free radicals generated by PpIX and ROSs, and either stimulates nerve endings directly or mediates pain through inflammatory by-products.[35–37]

To verify the effectiveness of PDMN-PDT in anti-tumor treatment, we divided mouse models of squamous cell carcinoma into different experimental groups based on the method of drug application and drug incubation time (1.5 and 4 h) (Figure 4A). Drug delivery methods included topical application, application with US, application with MA, and application with PDMN. Considering the superior transdermal permeation effect of PDMN, the concentration of 5-ALA was reduced from 20% to 10%, which potentially lowered the cost of the medication to reduce the economic burden. The PDMN-PDT (4 h) group exhibited significantly better tumor suppression than the other groups. The tumor-suppressive effect of the PDMN-PDT (1.5 h) group was comparable with that of the MA-PDT (4 h) and US-PDT (4 h) groups (Figures 4D and 4E). H&E staining provided corroborative evidence for this hypothesis (Figure 4G). To further determine the production of ROSs and ensure safety, we evaluated the PpIX levels in the tumors, skin, and blood of each experimental group after a single treatment (Figure 4F). The results showed that PDMN did not cause a significant increase in

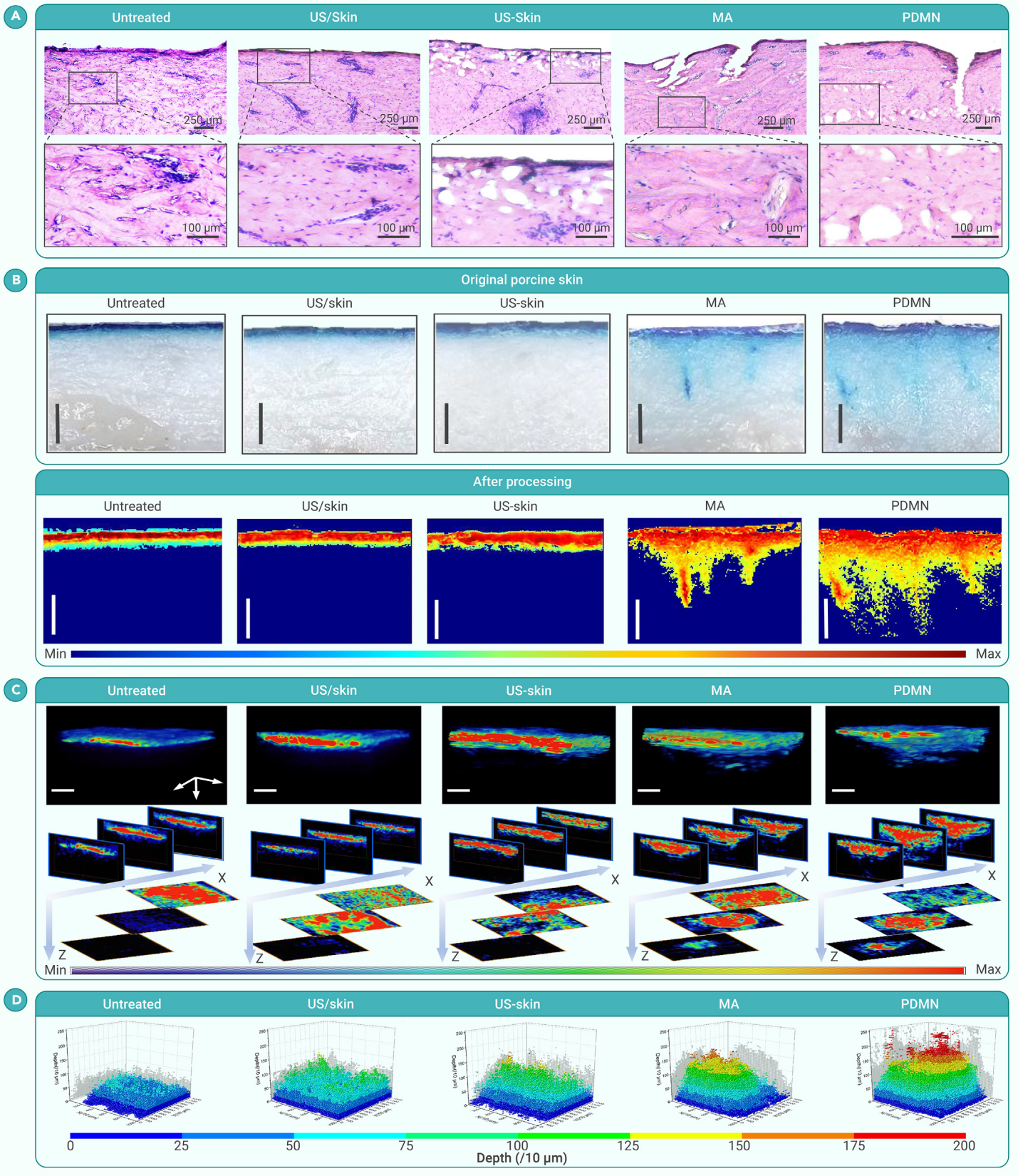

Figure 3. PDMN platform for efficient transdermal drug delivery (A) Representative H&E staining images of porcine skin under different treatments. (B) 2D side view of MB permeation of porcine skin (top) and after image processing (bottom). Scale bar, 1 mm. (C) 3D TTD images of MB delivery of five groups. Scale bar, 1 mm. (D) Distributions of pixel points of TTD images in the depth direction. Here, the maximum pixel values for each column of TTD intensity were selected and aligned in the same row. Then, effective pixel coordinates were extracted using a threshold of 0.1 times the peak intensity and plotted in a 3D scatterplot.

PpIX levels on the skin surface or in blood circulation. Based on the quantification of PpIX levels in the tumors, skin, and blood before (Figure 4C) and after (Figure 4F) combined PDT, we concluded that PDMN-mediated rapid drug delivery can achieve efficient PDT without increasing the risk of adverse effects (Figure S8). Moreover, in comparison with the other groups with a 4-h incubation time, PDMN-PDT with 1.5 h of incubation showed similar drug penetration

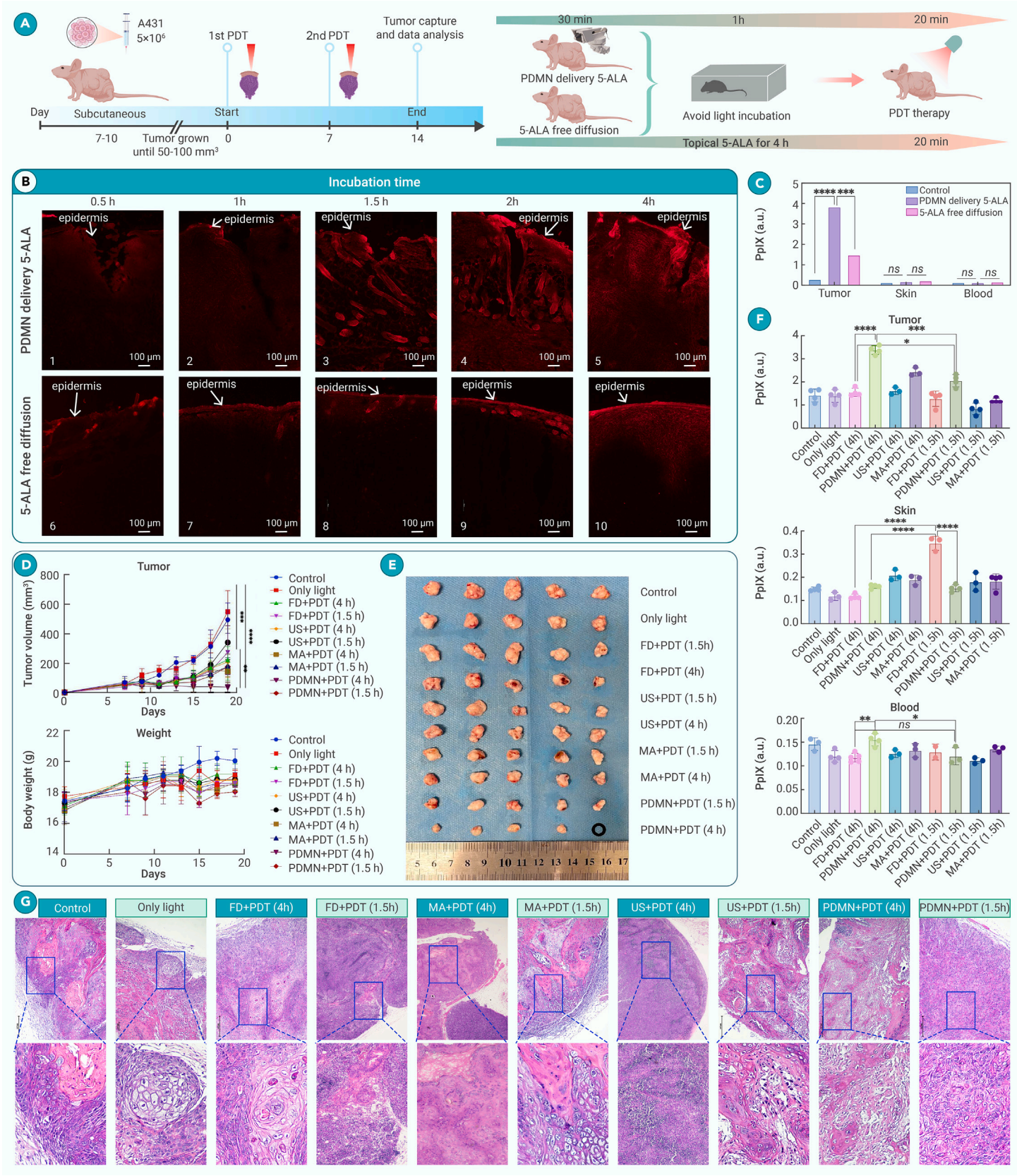

Figure 4. PDMN-PDT in A431 murine models (A) Schematic diagram of nude mice with squamous cell carcinoma *in vivo* and experiment protocol. (B) Image of PpIX fluorescence intensity in nude mouse skin after PDMN delivery of 5-ALA and topical administration of 5-ALA (the red color represents fluorescence of PpIX with fluorescence peaks at 630–650 nm). 1–5 represent PDMN delivery of 5-ALA for 0.5, 1, 1.5, 2, and 4 h and 6–10 represent 5-ALA free diffusion for 0.5, 1, 1.5, 2, and 4 h. Scale bar, 100 μm. (C) PpIX intensity in the tumor, skin, and blood in PDMN drug delivery strategy and free diffusion after 4 h, respectively (n = 3 independent samples). (D) Changes in tumor volume and body weight of A431 tumor-bearing mice after treatment (n = 5 independent samples). (E) Excised tumors at day 18 from five different mice (left to right) in each treatment group. (F) PpIX intensity in the tumor, skin, and blood after PDT treatment in different groups (n = 5 independent samples). (G) Representative images of H&E staining of mice skin after PDT treatment. Scale bar, 500 μm. Data are presented as mean ± SD, and statistical significance was analyzed via one-way ANOVA with Tukey's multiple comparison test. p values: *p < 0.05, **p < 0.01, ***p < 0.001, and ****p < 0.0001. FD, free diffusion.

Table 1. Comparison between PDMN-PDT and SS-PDT for viral warts

Item	PDMN-PDT (n = 21)	SS-PDT (n = 69)	p
Sex			
Male	13 (61.9)	32 (46.4)	0.213
Female	8 (38.1)	37 (53.6)	
Age (year)	30.14 ± 1.44	29.43 ± 1.56	0.811
Diagnosis			
Periungual warts	6 (28.6)	23 (33.3)	0.683
Plantar warts	15 (71.4)	46 (66.7)	
Response			
Excellent	11 (52.4)	53 (76.8)	
Good	9 (42.9)	11 (15.9)	0.033*
Poor	1 (4.8)	5 (7.3)	
Pain	3.90 ± 0.52	4.93 ± 0.29	0.089
Adverse events			
Bleeding	0 (0)	14 (20.3)	0.017*
Itching	0 (0)	9 (13.0)	0.080
Blister	0 (0)	3 (4.3)	0.446
DLQI[a]			
Pretreatment	11.19 ± 1.55	14.27 ± 0.58	0.074
Post-treatment	7.76 ± 1.34	4.25 ± 0.44	0.020
Total time (min)	303.8 ± 15.0	600.0 ± 35.9	<0.0001*
Satisfaction[b]	9.38 ± 0.15	8.72 ± 0.16	0.003*
Recurrence	1 (4.8)	6 (8.7)	0.481

* $p < 0.05$.
[a]DQLI scores of 10 patients who underwent SS-PDT were not available.
[b]Satisfaction from 4 patients who underwent SS-PDT was not available.

efficiency and treatment efficacy. Therefore, we chose the 1.5-h incubation time condition for subsequent clinical trials.

Clinical trial: Evaluation of therapeutic efficacy in PDMN-mediated PDT for viral warts

After obtaining ethical approval, we conducted a clinical trial (ClinicalTrials.gov: NCT05488860) using PDMN-PDT to treat skin diseases (skin cancer and viral skin diseases). A total of 25 participants who provided informed consent completed PDMN-PDT in the Dermatology Outpatient Department of Xiangya Hospital between July 2022 and July 2023 (Figure S9; Table S1). Traditional PDT for viral warts is limited by low drug penetration efficiency and long incubation times resulting in poor treatment outcomes and a high economic burden for patients; therefore, PDT can serve only as a secondary treatment option for viral warts.[38–41] To enhance the efficacy of PDT, we previously reported the use of superficial shaving (SS), an invasive pretreatment method, to remove the hyperkeratotic layer and increase drug penetration efficiency, followed by PDT treatment (SS-assisted PDT).[42] Although some improvements were achieved, SS-assisted PDT caused side effects, including bleeding, pain, and susceptibility to infection. As PDMN can significantly enhance the penetration of 5-ALA, we believe that PDMN-PDT may be a potentially effective treatment for human papilloma virus-infected warts. We compared PDMN-PDT with the previously reported SS-assisted PDT (Figure S10). Notably, the 5-ALA concentration in the PDMN group was half of that in the SS group, and the incubation times were 1.5 and 4 h for the PDMN and SS groups, respectively. Additionally, no anesthesia was administered in the PDMN group, whereas it was administered in the SS group. As shown in Table 1, the PDMN group exhibited a higher response rate compared to the SS group (95.3% vs. 92.7%, p = 0.033), demonstrating efficient drug penetration and improved treatment effectiveness with PDMN. The pain score in the PDMN group was comparable with that in the SS group even without the use of anesthesia (3.90 ± 0.52 vs. 4.93 ± 0.29, p = 0.089), thus highlighting the pain-reducing effects of PDMN. Additionally, the absence of post-treatment side effects, such as bleeding (0% vs. 20.3%, p = 0.017), itching (0% vs. 13.0%, p = 0.080), and blisters (0% vs. 4.3%, p = 0.446), in the PDMN group indicated the safety of this method. After PDMN-PDT, the Dermatology Life Quality Index of the patients decreased from 11.19 ± 1.55 to 7.76 ± 1.34 (p = 0.041). This statistically significant decrease demonstrates the effectiveness of PDMN in improving the life quality of patients. Furthermore, PDMN significantly reduced the total treatment time (303.8 ± 15.0 vs. 600.0 ± 35.9, $p < 0.0001$) owing to the improved drug penetration efficiency and treatment effectiveness. Overall, patients in the PDMN group reported higher satisfaction scores (9.38 ± 0.15 vs. 8.72 ± 0.16, p = 0.003), indicating superior therapeutic outcomes. The above experimental results demonstrate that as a transdermal drug delivery method, PDMN are effective for increasing drug penetration efficiency and treatment effectiveness, reducing side effects, and relieving pain in clinical practice. Moreover, they can reduce the economic burden on patients and improve patient satisfaction and compliance by reducing the required drug concentration and treatment time.

To provide a more intuitive demonstration of the therapeutic effects of PDMN, we present several typical cases (Figure 5A). Case 001 was a 26-year-old man with a 3-year history of multiple plantar warts on his left second toe resulting in complaints of pain and discomfort during ambulation. Previous treatment modalities involving cryotherapy and laser therapy were ineffective, leading to frequent recurrences. According to the protocol, the treatment was repeated every 2 weeks for a total of four sessions, resulting in complete resolution of the plantar wart after 1 month (Figure 5B). The patient did not report any side effects such as swelling, erythema, or blisters. No recurrence was detected during the follow-up until July 15, 2023. Cases 005 and 008 were both diagnosed with periungual warts and had previously received conventional treatment with poor efficacy. Treatment with PDMN was administered for three and two sessions, respectively, resulting in complete resolution of the cutaneous lesions (Figure 5C). In case 008, the patient presented with lesions on both hands, and only the left-hand lesion was initially selected for experimental treatment (Figure 5D). However, after the two treatments, the lesions on both hands disappeared, possibly indicating a remote effect of PDMN in conjunction with PDT or an associated immune response (Figure S11). Case 015 also demonstrated the remote effect of PDMN-PDT (Figure 5E). Only the lesions within the dashed box received treatment, but the three surrounding lesions also showed significant improvement, which may indicate a potential enhancement of the immune response. The above case demonstrates the significant effect of PDMN in treating stubborn viral warts and suggests that PDMN may enhance the immune response.

Clinical trial: Evaluation of therapeutic efficacy in PDMN-mediated PDT for skin cancer

To evaluate the effect of PDMN on anti-tumor therapy, we designed a self-controlled trial with ethical approval for patients with extramammary Paget's disease (EMPD). Being a malignant skin tumor, EMPD is conventionally treated by surgical excision, which often results in severe trauma, pain, and risk of infection.[43] Although according to expert consensus, EMPD is an indication of PDT, some studies have indicated that PDT is not significantly effective in treating EMPD. Our case report describes the successful treatment of a 75-year-old man with EMPD using PDMN-PDT. The patient had experienced red patches in his right axillary area for 3 years, accompanied by pruritus, which affected his sleep and quality of life. The pathological diagnosis was confirmed as EMPD. Despite the administration of the aforementioned treatments, the lesions exhibited an exacerbating trend, progressing circumferentially while concurrently eliciting pruritus. The lesion was divided into upper and lower halves. The upper half was treated with conventional PDT (20% 5-ALA, 4-h incubation), whereas the lower half was treated with PDMN-mediated PDT (10% 5-ALA, 1.5-h incubation) (Figure 6A). After treatment once per week for a total of 5 weeks, the results showed that treatment with PDMN-PDT significantly improved the skin lesions, with erythema nearly disappearing and slight hyperpigmentation (Figure 6B). Pathological analysis of the lesions revealed no residual Paget cells in the PDMN-PDT-treated areas, whereas

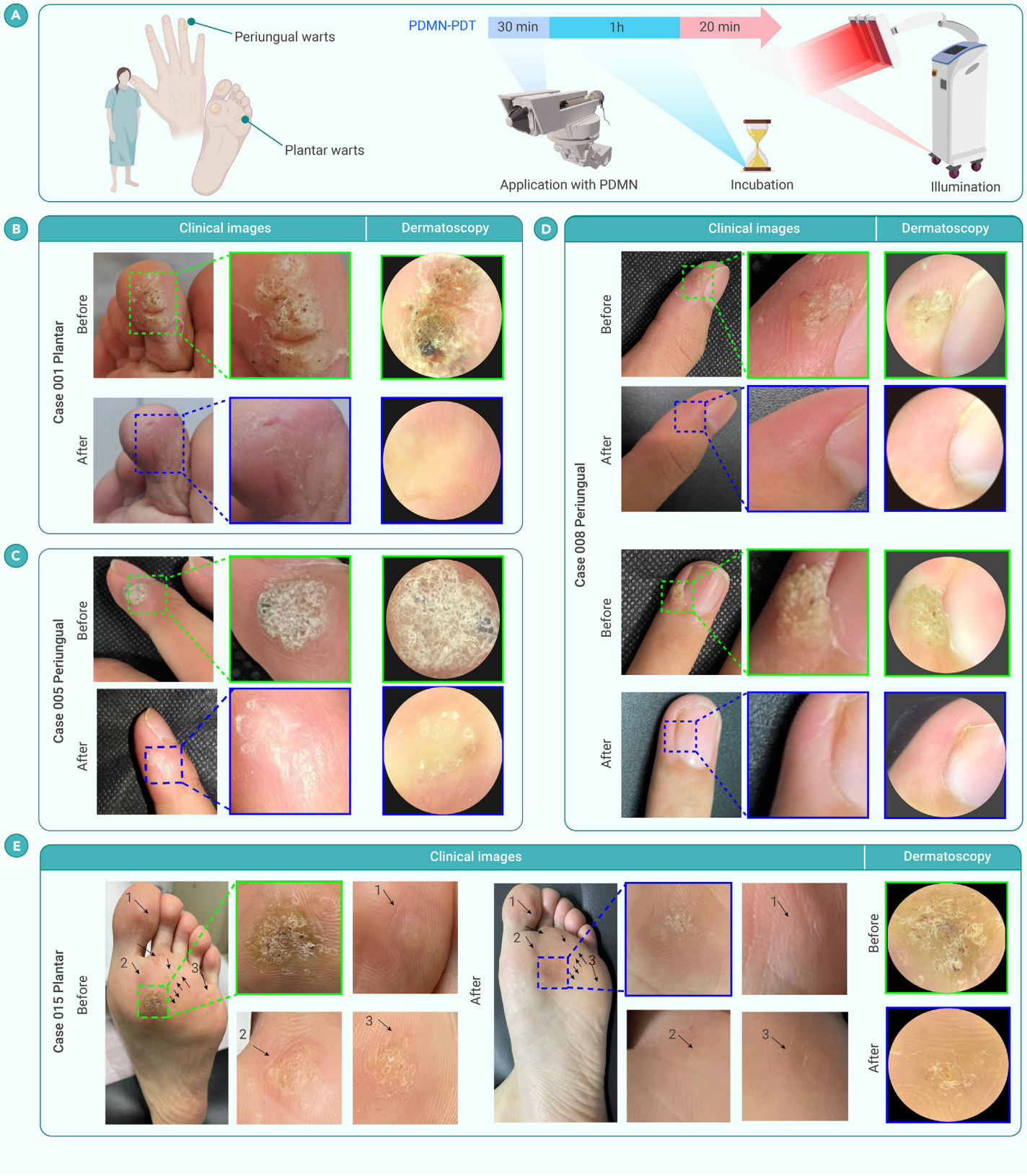

Figure 5. Clinical treatment of viral skin diseases (A) Clinical protocol for the treatment of viral warts. (B) Case 001 plantar wart patient: the top images show clinical photos before treatment, local magnification, and dermatoscopic images (on a black background), and the bottom images show clinical photos after PDMN combined with PDT treatment, local magnification, and dermatoscopic images (on a black background). (C and D) Images of case 005 (C) and case 008 (D) patient periungual warts, as described above. (E) Case 015 patient with multiple plantar warts. The treated areas are marked by dashed green lines. The lesions around the treated areas are marked by black arrows.

atypical Paget cells were observed in the epidermis and dermis treated with traditional PDT (Figure 6C). These results demonstrated that PDMN can effectively treat EMPD, thereby avoiding surgical trauma and side effects. During the follow-up period, the conventional-PDT-treated lesions recurred after 6 months, whereas the PDMN-PDT-treated-lesions showed no recurrence of infection (Figure 6D).

Additionally, we used PDMN-PDT in the treatment of BD (Figure 7A). PDT is also widely used in the treatment of BD.[41,44] In our case, a 34-year-old

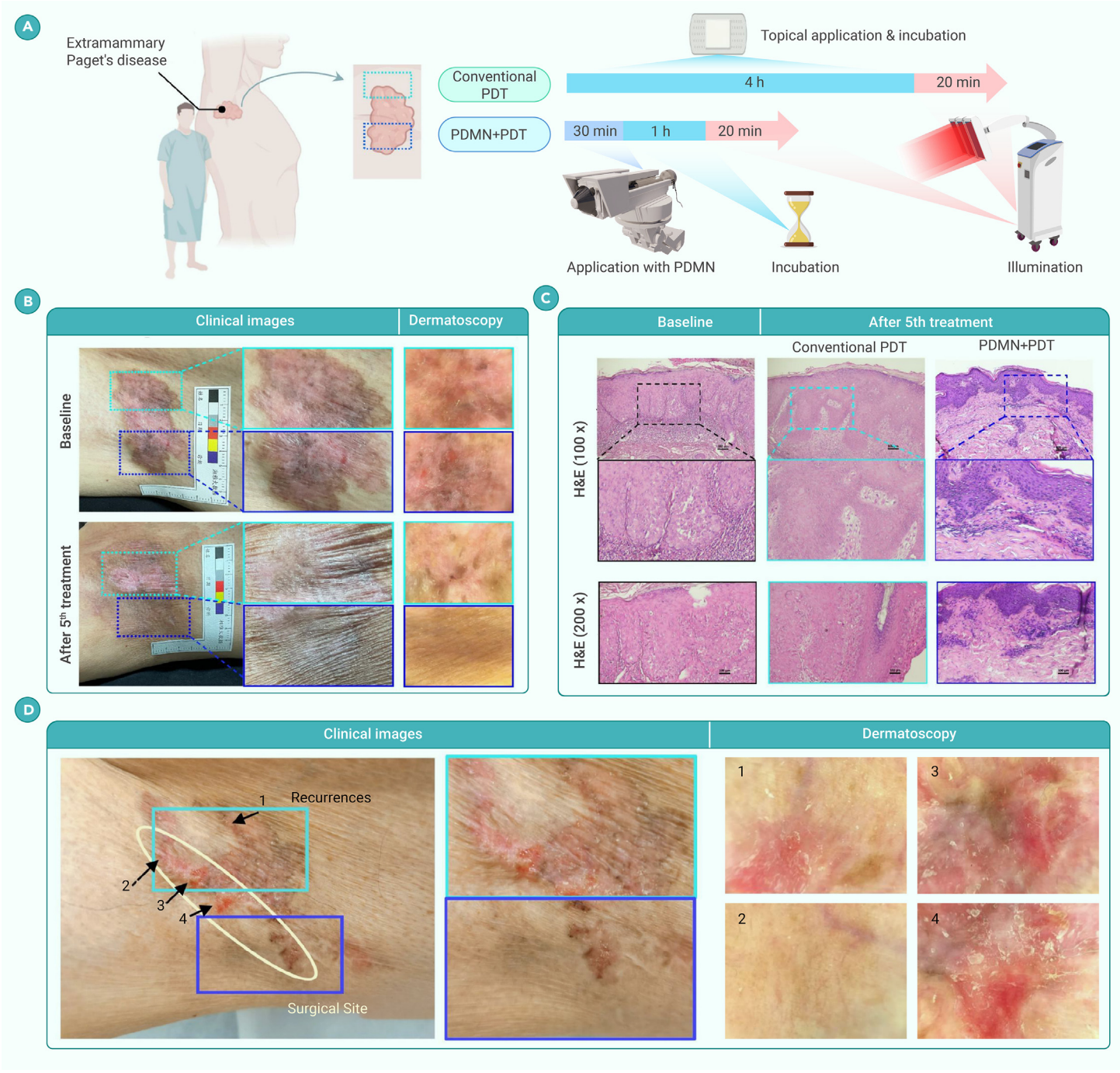

Figure 6. Clinical treatment of EMPD by PDMN-PDT (A) EMPD case presentation. Clinical protocol for the treatment of EMPD. (B) Comparison of traditional PDT (marked by a dashed green line) and PDMN-PDT (marked by a dashed blue line) in a patient with EMPD. The pre- and post-treatment clinical images and dermatoscopic images are shown. (C) Representative H&E images. Before treatment, numerous Paget cells, arranged in epidermal clusters, are distinctive for their large size, round shape, oval vesiculated nuclei, and abundant pale staining cytoplasm. Acanthosis is often present. After 5 treatments with traditional PDT (marked by a dashed green line), there are still a large number of Paget cells remaining. After 5 treatments with PDMN-PDT (marked by a dashed blue line), no residual Paget cells were seen (H&E; original magnification ×100). Scale bar, 100 μm. (D) Clinical images and dermatoscopic images of patient follow-up after 6 months.

female patient presented with red patches accompanied by scales and crust at the border between the thenar and hypothenar areas of her right hand for over a year. The lesions had clear borders, irregular shapes, and occasional itchiness. Cases in which BD manifests in the periungual area, fingers, and palms are considered less common. Dermoscopic images typically reveal pigment patterns characterized by non-structural pigmentation, along with the presence of brown dot-like or globular structures that exhibit a regular distribution.[41] The patient was enrolled in a self-controlled trial, and the lesions on the thenar area were treated with surgical excision followed by PDT, while the lesions on the hypothenar area were treated with PDMN-PDT. The concentration of 5-ALA used in both treatments was 10%. The results showed improvement and regression of both lesions, with a reduction in red patches, no scales, and the disappearance of subjective symptoms. Dermoscopy revealed the disappearance of vascular structures, indicating a clinical cure for the tumor. However, surgical excision combined with PDT treatment may result in scarring despite its advantages in controlling surgical margins and confirming the diagnosis. Additionally, when multiple or large skin lesions are present, surgical treatment may carry a risk of poor wound healing.

We also successfully confirmed the efficacy of PDMN-PDT in treating another case of cutaneous lymphangioma circumscriptum (CLC) (Figure 7B).

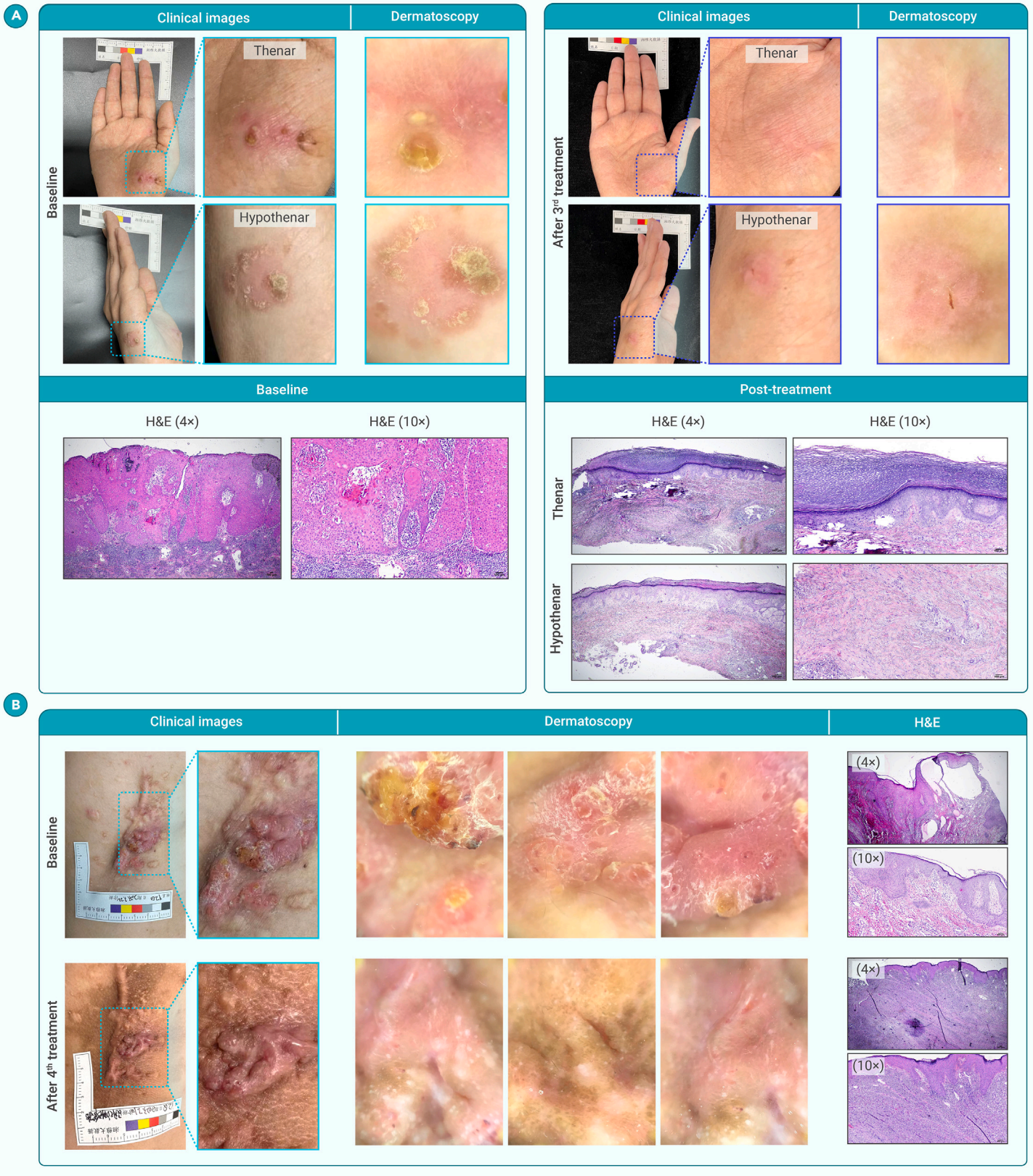

Figure 7. Clinical treatment of BD and CLC by PDMN-PDT (A) The pretreatment image: epidermal hyperkeratosis with parakeratosis, thickening of the spinous layer, elongation, and widening of the epidermal papillae with intact basal membrane. The spinous layer cells are disorganized, with a majority of cells showing significant atypia characterized by large and deeply stained nuclei, prominent nucleoli, and the presence of multinucleated giant cells, dyskeratotic cells, and pathological nuclear division phenomena. The post-treatment image: at the thenar of the lesion, there is thickening of the epidermis with excessive keratinization and incomplete cornification. The spinous layer is partially absent, with a few fibroblasts clustering and relatively thin collagen fibers. There is neovascularization and infiltration of inflammatory cells. In the hypothenar of the lesion, the skin tissue is close to normal. Scale bar, 100 μm. (B) The pretreatment image: crust, papillomatous hyperplasia, dilation, and congestion of superficial blood vessels and lymphatic vessels in the upper middle part of the dermis, infiltration of dense lymphocytes, plasma cells, and a few neutrophils in the dermis. The post-treatment image: the epidermis is intact and normal, with a normal arrangement of spinous layer cells. There are minimal dysplastic cells and no pathological mitotic figures observed. Scale bar, 100 μm.

A 22-year-old male patient had scar hypertrophy in the right axilla since childhood due to the surgical excision of a growth (specifics unknown). The scar hypertrophy continued to grow with age. Seven years ago, small vesicles the size of millet grains appeared around the scar in the right axilla. The vesicles gradually increased in number and size and were scattered or clustered and arranged in a belt-like pattern. The vesicles were not easily ruptured, had no apparent symptoms, and were left untreated. One year ago, the vesicles rapidly increased in number. Dermatological examination after enrollment showed that millet- to pea-sized vesicles were visible in the right axilla clustered in groups resembling frog eggs and some rashes merged, with thick vesicle walls, white translucent or purplish-red vesicular fluid, and easy bleeding upon touch. Upon microscopy examination, pale purple cavity-like structures were observed. After receiving PDMN-PDT treatment for 4 sessions, the results showed the disappearance of the clustered vesicles, leaving only dark red pigmentation and scars, without bleeding, exudation, or significant subjective symptoms. Skin microscopy examination showed that the locally diffused pale purple cavity-like structures disappeared, leaving pigmentation. Therefore, PDMN-PDT has enormous potential for tumor therapy and may reduce side effects.

DISCUSSION

In this work, we developed a PDMN platform and a new treatment method, PDMN-PDT, for skin disease therapy. The advances of the PDMN platform were validated by MB and 5-ALA delivery *in vitro* and *in vivo* resulting in deep dermis cavitation and enhanced transdermal drug delivery. The PDMN platform generated fractional US to achieve deep dermis cavitation and induce the generation of local PpIX. Compared with other US-mediated sonodynamic or PDT devices,[45–47] which usually require the use of sonosensitizers for enhancement or the utilization of nanoparticles to increase penetration depth, the PDMN platform eliminates the need for any modification of the drug properties,[48] thereby avoiding the complexity of drug modification procedures and ensuring the stability of the drug's chemical structure. Moreover, compared to microneedle patches, PDMN can regulate the dermal skin tissue structure and further accelerate drug penetration rates as an external trigger. As a transdermal drug delivery system (TDDS), PDMN platform's functions and advantages are universal for almost all topical medications, making it poised for excellent prospects in the field of topical therapy within the pharmaceutical market. As a TDDS, the PDMN platform holds significant value in the market. The global TDDS market was valued at USD $59.4 billion in 2022 and is expected to expand at a compound annual growth rate (CAGR) of 11.9% from 2023 to 2030.[49–51] However, current transdermal drug delivery devices are flawed; the associated issues include long operation times, damage caused to the skin, limited drug application, low diffusion efficacy, and so on.[52] The PDMN platform proposed in this article can directly deliver therapeutic agents to topical lesions with enhanced bioavailability and reduced adverse effects, which shows the successful overcoming of some disadvantages that exist in current TDDSs. From a clinical perspective, PDT has been described as an effective anti-infection and anti-cancer therapeutic technology.[53] The global PDT market is estimated to have grown from USD $4.58 billion in 2022 to $5.29 billion in 2023 at a CAGR of 15.5%. PDT is cost intensive, as it involves specialized equipment, photosensitive drugs, and skilled personnel, which partially leads to its limited application.[54] The PDMN platform can reduce the costs of PDT by improving drug efficiency and shortening treatment duration (reducing indirect medical costs, including those for travel and accommodation). In our trials, PDMN-PDT successfully cured viral warts, EMPD, BD, and CLC. Moreover, compared to those in conventional PDT, the treatment duration was shorter, the drug concentration was lower, and the procedure was non-invasive, leading to high patient compliance and economic benefits.

In terms of safety considerations, the skin recovery after treatment with the PDMN platform was simply evaluated by observing the surface appearance of skin damage on nude mice and patients (Figure S12). The micropores had significantly diminished within 5 min, and the skin showed complete recovery 30 min post-insertion. After treatment, there were no obvious side effects except for some visible micropores and local erythema at the insertion site. The operating frequency of the PDMN is 114 kHz, which is a relatively safe value with a 3 W/cm^2 intensity. Its safety can be assured, as the intensities of the majority of sonophoresis applications remain below 3.5 W/cm^2. In the animal experiment, the mice in the PDMN group did not exhibit significant weight loss or decreased lifespan compared with the control group. In the clinical trial, patients reported slight side effects such as edema and pain, similar to those observed with traditional PDT treatment. As of November 20, 2023, no suspected PDMN-related adverse effects were reported by the patients during follow-up. The main limitation is that the current device can only generate a small area of fractional US with a 5 × 5 mm MA, making it unsuitable for large or multifocal lesions. In addition, the recurrence rate of cases treated with PDMN requires long-term follow-up studies to evaluate. Further study should focus on the molecular-level biological effects of the PDMN platform and its long-term safety.

MATERIALS AND METHODS

Materials and methods related to this work are available in the supplemental information.

REFERENCES

1. Kabashima, K., Honda, T., Ginhoux, F., et al. (2019). The immunological anatomy of the skin. Nat. Rev. Immunol. ***19***(1): 19–30. https://doi.org/10.1038/s41577-018-0084-5.
2. Prausnitz, M.R., and Langer, R. (2008). Transdermal drug delivery. Nat. Biotechnol. ***26***(11): 1261–1268. https://doi.org/10.1038/nbt.1504.
3. Li, X., Lovell, J.F., Yoon, J., et al. (2020). Clinical development and potential of photothermal and photodynamic therapies for cancer. Nat. Rev. Clin. Oncol. ***17***(11): 657–674. https://doi.org/10.1038/s41571-020-0410-2.
4. Simões, M.C.F., Sousa, J.J.S., and Pais, A.A.C.C. (2015). Skin cancer and new treatment perspectives: A review. Cancer Lett. ***357***(1): 8–42. https://doi.org/10.1016/j.canlet.2014.11.001.
5. Barr, H., Kendall, C., Bazant-Hegemark, F., et al. (2006). Endoscopic photodynamic therapy for oesophageal disease. Photodiagnosis Photodyn. Ther. ***3***(2): 102–105. https://doi.org/10.1016/j.pdpdt.2006.03.008.
6. Buttar, N.S., Wang, K.K., Lutzke, L.S., et al. (2001). Combined endoscopic mucosal resection and photodynamic therapy for esophageal neoplasia within Barrett's esophagus. Gastrointest. Endosc. ***54***(6): 682–688. https://doi.org/10.1067/mge.2001.119875.
7. Schroeder, A., Kost, J., and Barenholz, Y. (2009). Ultrasound, liposomes, and drug delivery: principles for using ultrasound to control the release of drugs from liposomes. Chem. Phys. Lipids ***162***(1-2): 1–16. https://doi.org/10.1016/j.chemphyslip.2009.08.003.
8. Polat, B.E., Deen, W.M., Langer, R., et al. (2012). A physical mechanism to explain the delivery of chemical penetration enhancers into skin during transdermal sonophoresis - Insight into the observed synergism. J. Contr. Release ***158***(2): 250–260. https://doi.org/10.1016/j.jconrel.2011.11.008.
9. Sonokawa, T., Matsumoto, M., Takegahara, K., et al. (2021). Usefulness of simultaneous type image-enhanced endoscope system in photodynamic therapy for centrally located lung cancer. Photodiagnosis Photodyn. Ther. ***35***: 102345. https://doi.org/10.1016/j.pdpdt.2021.102345.
10. Zhu, Z., Wang, J., Pei, X., et al. (2023). Blue-ringed octopus-inspired microneedle patch for robust tissue surface adhesion and active injection drug delivery. Sci. Adv. ***9***(25): h2213. https://doi.org/10.1126/sciadv.adh2213.
11. Hu, C., He, X., Chen, Y., et al. (2021). Metformin mediated PD-L1 downregulation in combination with photodynamic-immunotherapy for treatment of breast cancer. Adv. Funct. Mater. ***31***(11): 2007149. https://doi.org/10.1002/adfm.202007149.
12. Huang, Z. (2005). A review of progress in clinical photodynamic therapy. Technol. Cancer Res. Treat. ***4***(3): 283–293. https://doi.org/10.1177/153303460500400308.
13. Petukhova, T.A., Hassoun, L.A., Foolad, N., et al. (2017). Effect of expedited microneedle-assisted photodynamic therapy for field treatment of actinic keratoses. A randomized clinical trial. JAMA Dermatol. ***153***(7): 637–643. https://doi.org/10.1001/jamadermatol.2017.0849.
14. Zhi, D., Yang, T., O'Hagan, J., et al. (2020). Photothermal therapy. J. Contr. Release ***325***: 52–71. https://doi.org/10.1016/j.jconrel.2020.06.032.
15. Mitragotri, S., Farrell, J., Tang, H., et al. (2000). Determination of threshold energy dose for ultrasound-induced transdermal drug transport. J. Control Release ***63***(1-2): 41–52. https://doi.org/10.1016/S0168-3659(99)00178-9.
16. Polat, B.E., Hart, D., Langer, R., et al. (2011). Ultrasound-mediated transdermal drug delivery: Mechanisms, scope, and emerging trends. J. Control Release ***152***(3): 330–348. https://doi.org/10.1016/j.jconrel.2011.01.006.
17. Seah, B.C.Q., and Teo, B.M. (2018). Recent advances in ultrasound-based transdermal drug delivery. Int. J. Nanomed. ***13***: 7749–7763. https://doi.org/10.2147/IJN.S174759.
18. Rwei, A.Y., Paris, J.L., Wang, B., et al. (2017). Ultrasound-triggered local anaesthesia. Nat. Biomed. Eng. ***1***(8): 644–653. https://doi.org/10.1038/s41551-017-0117-6.
19. Cao, Z., Yuan, G., Zeng, L., et al. (2022). Macrophage-targeted sonodynamic/photothermal synergistic therapy for preventing atherosclerotic plaque progression using CuS/TiO2 heterostructured nanosheets. ACS Nano ***16***(7): 10608–10622. https://doi.org/10.1021/acsnano.2c02177.
20. Hao, Y., Dong, M., Zhang, T., et al. (2017). Novel approach of using near-infrared responsive PEGylated gold nanorod coated poly(l-lactide) microneedles to enhance the antitumor efficiency of docetaxel-loaded MPEG-PDLLA micelles for treating an A431 tumor. ACS Appl. Mater. Interfaces ***9***(8): 15317–15327. https://doi.org/10.1021/acsami.7b03604.
21. Mitsuishi, T., Sasagawa, T., Kato, T., et al. (2010). Combination of carbon dioxide laser therapy and artificial dermis application in plantar warts: human papillomavirus DNA analysis after treatment. Dermatol. Surgery (St Louis) ***36***(9): 1401–1405.

22. You, J., Yang, C., Han, J., et al. (2023). Ultrarapid-acting microneedles for immediate delivery of biotherapeutics. Adv. Mater. ***35***(45): 2304582. https://doi.org/10.1002/adma.202304582.
23. Zhang, Y., Wang, S., Yang, Y., et al. (2023). Scarless wound healing programmed by core-shell microneedles. Nat. Commun. ***14***(1): 3431. https://doi.org/10.1038/s41467-023-39129-6.
24. Zhang, Y., Xu, Y., Kong, H., et al. (2023). Microneedle system for tissue engineering and regenerative medicine. Explorations ***3***(1): 20210170. https://doi.org/10.1002/EXP.20210170.
25. Zhang, X., Chen, G., Wang, Y., et al. (2024). Spatial tumor biopsy with fluorescence PCR microneedle array. Innovation ***5***(1): 100538. https://doi.org/10.1016/j.xinn.2023.100538.
26. Park, J.M., Jeong, K.H., Bae, M.I., et al. (2016). Fractional radiofrequency combined with sonophoresis to facilitate skin penetration of 5-aminolevulinic acid. Laser Med. Sci. ***31***(1): 113–118. https://doi.org/10.1007/s10103-015-1835-1.
27. Liu, P., Fu, Y., Wei, F., et al. (2022). Microneedle Patches with O_2 propellant for deeply and fast delivering photosensitizers: towards improved photodynamic therapy. Adv. Sci. ***9***(25): 2202591. https://doi.org/10.1002/advs.202202591.
28. Zhu, J., Dong, L., Du, H., et al. (2019). 5-Aminolevulinic acid-loaded hyaluronic acid dissolving microneedles for effective photodynamic therapy of superficial tumors with enhanced long-term stability. Adv. Healthcare Mater. ***8***(22): 1900896. https://doi.org/10.1002/adhm.201900896.
29. Tepole, A.B., Kabaria, H., Bletzinger, K.U., et al. (2015). Isogeometric Kirchhoff-Love shell formulations for biological membranes. Comput. Methods Appl. Math. ***293***: 328–347. https://doi.org/10.1016/j.cma.2015.05.006.
30. Dollet, B., Marmottant, P., and Garbin, V. (2019). Bubble dynamics in soft and biological matter. Annu. Rev. Fluid Mech. ***51***: 331–355. https://doi.org/10.1146/annurev-fluid-010518-040352.
31. Holzapfel, G.A., Gasser, T.C., and Ogden, R.W. (2000). A new constitutive framework for arterial wall mechanics and a comparative study of material models. J. Elasticity ***61***(1-3): 1–48. https://doi.org/10.1023/A:1010835316564.
32. Wang, Y., Zhang, R., Pu, Y., et al. (2023). Sample collection, DNA extraction, and library construction protocols of the human microbiome studies in the international human phenome project. Phenomics ***3***(3): 300–308. https://doi.org/10.1007/s43657-023-00097-y.
33. Shan, H., Sun, X., Liu, X., et al. (2023). One-step formation of targeted liposomes in a versatile microfluidic mixing device. Small ***19***(7): 2205498. https://doi.org/10.1002/smll.202205498.
34. Xie, Y., Wu, H., Chen, Z., et al. (2023). Non-invasive evaluation of transdermal drug delivery using 3-D transient triplet differential (TTD) photoacoustic imaging. Photoacoustics ***32***: 100530. https://doi.org/10.1016/j.pacs.2023.100530.
35. Ubbink, R., Prens, E.P., and Mik, E.G. (2021). Quantitative intracellular oxygen availability before and after 5-aminolevulinic acid skin photodynamic therapy. Photodiagnosis Photodyn. Ther. ***36***: 102599. https://doi.org/10.1016/j.pdpdt.2021.102599.
36. Picard, M. (2022). Why Do We Care More About Disease than Health? Phenomics ***2***(3): 145–155. https://doi.org/10.1007/s43657-021-00037-8.
37. Ang, J.M., Riaz, I.B., Kamal, M.U., et al. (2017). Photodynamic therapy and pain: A systematic review. Photodiagnosis Photodyn. Ther. ***19***: 308–344. https://doi.org/10.1016/j.pdpdt.2017.07.002.
38. Wang, B., Shi, L., Zhang, Y.F., et al. (2017). Gain with no pain? Pain management in dermatological photodynamic therapy. Br. J. Dermatol. ***177***: 656–665.
39. Sterling, J.C., Gibbs, S., Haque Hussain, S.S., et al. (2014). British Association of Dermatologists' guidelines for the management of cutaneous warts 2014. Br. J. Dermatol. ***171***(3): 696–712. https://doi.org/10.1111/bjd.15344.
40. Viennet, C., Gheit, T., Muret, P., et al. (2013). Assessment of the efficacy of a new formulation for plantar wart mummification: new experimental design and human papillomavirus identification. Clin. Exp. Dermatol. ***38***(1): 85–88. https://doi.org/10.1111/ced.12025.
41. Champeau, M., Vignoud, S., Mortier, L., et al. (2019). Photodynamic therapy for skin cancer: How to enhance drug penetration? J. Photochem. Photobiol. B ***197***: 111544. https://doi.org/10.1016/j.jphotobiol.2019.111544.
42. Wu, L., Chen, W., Su, J., et al. (2019). Efficacy of the combination of superficial shaving with photodynamic therapy for recalcitrant periungual warts. Photodiagnosis Photodyn. Ther. ***27***: 340–344. https://doi.org/10.1016/j.pdpdt.2019.06.021.
43. Kibbi, N., Owen, J.L., Worley, B., et al. (2022). Evidence-based clinical practice guidelines for Extramammary Paget Disease. JAMA Oncol. ***8***(4): 618–628. https://doi.org/10.1001/jamaoncol.2021.7148.
44. Agostinis, P., Berg, K., Cengel, K.A., et al. (2011). Photodynamic therapy of cancer: An update. CA A Cancer J. Clin. ***61***(4): 250–281. https://doi.org/10.3322/caac.20114.
45. Kearney, M.C., Brown, S., Donnelly, R.F., et al. (2014). Potential of microneedles in enhancing delivery of photosensitizing agents for photodynamic therapy. Photodiagnosis Photodyn. Ther. ***11***(4): 459–466. https://doi.org/10.1016/j.pdpdt.2014.09.003.
46. Dai, H., Shen, Q., Shao, J., et al. (2021). Small molecular NIR-II fluorophores for cancer phototheranostics. Innovation ***2***(1): 100082. https://doi.org/10.1016/j.xinn.2021.100082.
47. Karimkhani, C., Dellavalle, R.P., Coffeng, L.E., et al. (2017). Global skin disease morbidity and mortality: An update from the global burden of disease study 2013. JAMA Dermatol. ***153***(5): 406–412. https://doi.org/10.1001/jamadermatol.2016.5538.
48. Braathen, L.R., Szeimies, R.M., Basset-Seguin, N., et al. (2007). Guidelines on the use of photodynamic therapy for nonmelanoma skin cancer: An international consensus. J. Am. Acad. Dermatol. ***56***(1): 125–143. https://doi.org/10.1016/j.jaad.2006.06.006.
49. Jeong, W.Y., Kwon, M., Choi, H.E., et al. (2021). Recent advances in transdermal drug delivery systems: A review. Biomater. Res. ***25***(1): 24. https://doi.org/10.1186/s40824-021-00226-6.
50. Huang, D., Wang, J., Song, C., et al. (2023). Ultrasound-responsive matters for biomedical applications. Innovation ***4***(3): 100421. https://doi.org/10.1016/j.xinn.2023.100421.
51. Songca, S.P. (2023). Combinations of photodynamic therapy with other minimally invasive therapeutic technologies against cancer and microbial infections. Int. J. Mol. Sci. ***24***(13): 10875. https://doi.org/10.3390/ijms241310875.
52. Prausnitz, M.R., Mitragotri, S., and Langer, R. (2004). Current status and future potential of transdermal drug delivery. Nat. Rev. Drug Discov. ***3***(2): 115–124. https://doi.org/10.1038/nrd1304.
53. Dolmans, D.E.J.G.J., Fukumura, D., and Jain, R.K. (2003). Photodynamic therapy for cancer. Nat. Rev. Cancer ***3***(5): 380–387. https://doi.org/10.1038/nrc1071.
54. Li, X., Gu, L., Chen, Y., et al. (2022). A novel 450-nm laser-mediated sinoporphyrin sodium-based photodynamic therapy induces autophagic cell death in gastric cancer through regulation of the ROS/PI3K/Akt/mTOR signaling pathway. BMC Med. ***20***(1): 475. https://doi.org/10.1186/s12916-022-02676-8.

ACKNOWLEDGMENTS

This work was supported by the Department of Science and Technology of Hunan Province, High-tech Industry Science and Technology Innovation Leading Program (grant 2020SK2003 to Z.C.); the Science Fund for Distinguished Young Scholars of Hunan Province (grant 2021JJ10069 to Z.C.); Mobile Healthcare: Ministry of Education, China Mobile Joint Laboratory (grant CMCMII-202200349 to S.Z.); and the National Natural Science Foundation of China (grant 2022YFC2504700 to X.C.). We would also like to thank Mr. Zherui Liu (The University of Manchester, Manchester, UK) for graphical guidance.

AUTHOR CONTRIBUTIONS

Zeyu Chen, H.P., S.Z., and X.C. conceptualized the idea. X.L., Ziyan Chen, and L.W. designed the experiment. S.Z., Z.L., M.Z., J.S., Y.T., and J.L. recruited and allocated the patients for clinical trials. Experimental operation and data acquisition: X.L., Ziyan Chen, H.W., L.P., and X.W. completed the animal experiment and data collection. X.L., H.W., Ziyan Chen, and Z.J. completed the clinical trial and data collection. X.L., Ziyan Chen, and Z.J. analyzed and interpreted the data. Y.X., H.S., Q.L., H.P., and T.Y. provided technical support. Ziyan Chen, X.L., and Z.J. conducted visualization. S.Z., Zeyu Chen, and X.C. acquired funding. X.C. administrated the project. Ziyan Chen and X.L. wrote the manuscript. S.Z., Zeyu Chen, Z.J., H.S., H.P., and X.C. provided major revisions.

DECLARATION OF INTERESTS

The authors declare no competing interests.

SUPPLEMENTAL INFORMATION

Supplemental information can be found online at https://doi.org/10.1016/j.xinn.2024.100621.

LEAD CONTACT WEBSITE

https://www.csu.edu.cn/